Light Scattering Analysis of Fibril Growth from the Amino-terminal Fragment β(1–28) of β-Amyloid Peptide

Chih-Lung Shen,* Grayson L. Scott,‡ Farah Merchant,* and Regina M. Murphy*
*Department of Chemical Engineering and ‡Center for Health Sciences, University of Wisconsin, Madison, Wisconsin 53706 USA

ABSTRACT β-Amyloid protein (β-A/4) is the major protein component of Alzheimer disease-related senile plaques and has been postulated to be a significant contributing factor in the onset and/or progression of the disease. In the senile plaque, β-A/4 appears as bundles of amyloid fibrils. The biological activity of β-A/4 may be related to its state of aggregation. In this work, self-assembly, fibril formation, and interfibrillary aggregation of β(1–28), a synthetic peptide homologous with the amino-terminal fragment of β-A/4, were investigated. The predominant form of β(1–28) detected by size-exclusion chromatography and polyacrylamide gel electrophoresis was apparently a tetramer which does not bind Congo red. Aggregates containing cross-β sheet structures which bind Congo red and thioflavin T were observed at concentrations of approximately 0.3 mg/ml or greater. Concentrations of 0.5–1 mg/ml were necessary for aggregation into fibrils to be detectable by classical or quasielastic light scattering. Both fibril elongation and fibril-fibril aggregation occur over the time scale investigated. The kinetics of aggregation were much faster at physiological salt concentrations than at lower ionic strength. Ionic strength also appeared to influence the morphology of the fibril aggregates. The data indicate that sample preparation method and sample history influence fibril size and number density.

INTRODUCTION

β-Amyloid protein (β-A/4) has been identified as the major protein component of neuritic plaques and cerebrovascular amyloid deposits in patients with Alzheimer's disease (Glenner and Wong, 1984; Wong et al., 1985; Masters et al., 1985). β-A/4 is a 39- to 43-residue proteolytic product of a normal membrane-associated precursor protein, with the shorter, more soluble form present in cerebrovascular deposits and the longer forms present in senile plaques (Prelli et al., 1988). The peptide contains an amino-terminal 28-residue domain which is extracellular in the precursor protein, and a carboxyl-terminal 11–15 residue domain which is part of the putative transmembrane domain of the precursor (Kang et al., 1987; Selkoe et al., 1988). β-A/4 deposits in senile plaques are organized as bundles of amyloid fibrils surrounded by abnormal neurites (Merz et al., 1981). The fibrils have an antiparallel β-sheet conformation and are conventionally detected by birefringence upon Congo red staining. Amorphous deposits of β-A/4 unaccompanied by neuritic damage have also been identified (Yamaguchi et al., 1989, 1990; Rozemuller et al., 1989).

β-A/4 has been proposed to be a major causative factor in the onset of Alzheimer's disease (Joachim and Selkoe, 1992). However, in vitro and in vivo assays of the biological activity of synthetic homologs of β-A/4 have given conflicting results (Whitson et al., 1989; Koh et al., 1990; Yankner et al., 1990; Kowall et al., 1991, 1992; Emre et al., 1992; Podlisny et al., 1992; Games et al., 1992; Rush et al., 1992; May et al., 1992; Malouf et al., 1992; Koo et al., 1993). The aggregation state of the peptide has recently been recognized as a potentially critical factor in determining the peptide's neurotoxic or neurotrophic activity (Cotman et al., 1992; Yankner, 1992). Neurotoxicity in in vivo studies has been correlated with the presence of large, Congo red-staining fibrillar deposits of injected synthetic peptides (Waite et al., 1992). In vitro studies showed that toxicity occurred only with "aged" peptides which have aggregated (Pike et al., 1991a, 1991b). Others have shown that "solubilizing" peptides enhances the susceptibility of treated cells to injury from excitotoxins (Mattson et al., 1992).

We report here investigations of amyloid fibril formation from a synthetic peptide, β(1–28), which is homologous to the amino-terminal sequence of β-A/4. Previous researchers have shown that β(1–28) adopts a random coil conformation at physiological conditions (Barrow and Zagorski, 1991) and spontaneously forms amyloid fibrils (Kirschner et al., 1987; Castano et al., 1986; Gorevic et al., 1987). In some (Whitson et al., 1989; Yankner et al., 1990) but not all (Pike et al., 1991b, Malouf et al., 1992) cases, β(1–28) has been shown to exert neurotrophic and/or neurotoxic effects in vitro. In work reported here, the kinetics of aggregation of β(1–28) were investigated. Light scattering and electron microscopy were used to characterize the rate and morphology of fibril elongation and interfibrillary aggregation. Effects of salt and peptide concentration were probed.

MATERIALS AND METHODS

Peptide Synthesis and Purification

A peptide homologous to the first 28 residues of β-A/4 (Kang et al., 1987) was synthesized and purified at the University of Wisconsin Biotechnology Center. The sequence is DAEFRHDSGYEVHHQKLVFFAEDVGSNK. The peptide was stepwise synthesized on the Applied Biosystems (Foster City, CA) automatic solid-phase peptide synthesizer. Stepwise coupling was greater than 99% based on the quantitative ninhydrin test. Unpurified pep-

Received for publication 12 July 1993 and in final form 2 September 1993.
Address reprint requests to Dr. Regina M. Murphy at the Department of Chemical Engineering, University of Wisconsin, 1415 Johnson Drive, Madison, WI 53706.

0006-3495/93/12/2383/13 $2.00

tide was lyophilized and stored at −70°C. The crude peptide was purified using reversed-phase high-pressure liquid chromatography (HPLC) on a 21.4 mm × 250 mm Dynamax-300 (Rainin, Woburn, MA) C_{18} column. To purify, the peptide was dissolved in 0.1% trifluoroacetic acid (TFA), applied to the column, and eluted in a gradient of 20–50% eluant B over 60 min (eluant A, 0.1% TFA; eluant B, 80% acetonitrile and 0.086% TFA). Purity was checked by analytical chromatography at a gradient of 20–50% eluant B on a 4.6 mm × 250-mm Vydac (Hesperica, CA) C_4 column. From the chromatograms, purity was estimated to be 95–99%. The recovered peptide was lyophilized and stored at −20°C in a dessicator. Mass spectroscopy analysis indicated that the peptide had a molecular weight of 3263 ± 1, compared to the expected molecular weight of 3262.

Circular dichroism spectroscopy

Circular dichroism (CD) spectra were obtained using a modified Cary Model 60 spectropolarimeter (On-line Instrument Systems, Bogart, GA). β(1–28) was prepared at a concentration of 0.2 mg/ml in 0.02 M phosphate buffer (K_2HPO_4/KH_2PO_4, pH 7.4, adjusted with NaOH). The peptide solution was filtered through a 0.45-μm Millipore (Bedford, MA) filter to remove dust and then placed into a vacuum system in order to discharge oxygen in the solution. A 0.1-cm quartz cell was used for far-UV (190–240 nm) measurements. The instrument was calibrated using D(+)-10-camphorsulfonic acid. Spectra were measured approximately 3 h after sample preparation. Ten scans each of duplicate samples were measured and averaged. Base line scans were run in duplicate, averaged, and then subtracted from the sample spectrum. The secondary structure was calculated from mean residue ellipticities using the secondary structural parameters reported by Chang (Chang et al., 1978).

Congo red absorbance spectroscopy

Congo red dye (Sigma, St. Louis, MO) was dissolved in PBSA (0.01 M K_2HPO_4/KH_2PO_4, 0.14 M NaCl, 0.02% NaN_3, pH 7.4) to a final concentration of 7 μM. β(1–28) was dissolved directly into the Congo red solution at 0.2–0.5 mg/ml and mixed gently at room temperature for 1 h. Spectrophotometric measurements from 700 to 300 nm were collected for each of the peptide-containing samples as well as for the free dye using a Hitachi (San Jose, CA) U-2000 UV-Vis spectrophotometer and a quartz cell having 1-cm path length (Klunk et al., 1989a, 1989b). Difference spectra were calculated by subtracting the free dye absorbance from the peptide-dye solution absorbance.

Thioflavin T fluorescence spectroscopy

Stock solutions of Thioflavin T (ThT, Sigma, St. Louis, MO) were prepared at 100 μM concentration. Lyophilized peptide was weighed and dissolved in 0.01 M phosphate buffer or PBSA. Peptide samples (0.8 ml) were incubated at room temperature for either 1 or 24 h, at which time 8-μl ThT stock solution was added (final ThT concentration, 1 μM). Fluorescence intensity was measured immediately after briefly vortexing the sample. Fluorescence measurements were obtained on a Model M-3 Alphascan (Photon Technology International, South Brunswick, NJ) spectrofluorometer. The sample chamber temperature was maintained at 25°C. Preliminary spectral measurements indicated that the peptide-dye mixture had an excitation maximum at 450 nm and an emission maximum at 482 nm and that the dye alone had essentially no fluorescence signal at these wavelengths, in agreement with reported literature values (Naiki et al., 1989; LeVine, 1993). These maxima were not a function of ionic strength. Therefore, all subsequent measurements were taken at an excitation wavelength of 450 nm and an emission wavelength of 482 nm. For each sample, ten measurements were taken and averaged; no increase in fluorescence during the measurement period was detected. Baseline fluorescence was measured for buffer containing the same quantity of ThT and subtracted.

HPLC

Size-exclusion HPLC experiments were conducted using the Waters (Millipore, Milford, MA) Model 625 LC system and the Waters Protein-Pak 125 column. PBSA was used as the mobile phase at a flow rate of 1.0 ml/min. Lyophilized β(1–28) was weighed and dissolved in either PBSA or 0.01 M phosphate buffer. Final concentrations were 0.2, 0.5, or 1.0 mg/ml; solution pH was 7.4. 10-μl samples were injected for each measurement and peaks were detected by absorbance at 280 nm. The column was calibrated with bovine serum albumin (67 kDa), ovalbumin (43 kDa), myoglobin (17 kDa), ribonuclease A (14 kDa), insulin (4.7 kDa), and guanosine (283 Da).

Sodium dodecyl sulfate-polyacrylamide gel electrophoresis (SDS-PAGE)

SDS-PAGE experiments were performed under nonreducing conditions using the Pharmacia (Uppsala, Sweden) pHastGel System and pHastGel high density homogeneous gels. Lyophilized peptide was weighed and dissolved in 0.01 M phosphate buffer, then diluted further with 0.01 M phosphate buffer containing NaCl, to a final peptide concentration of 1 or 0.5 mg/ml and a final NaCl concentration of 0.14 M. Solutions were mixed with SDS to give a final SDS concentration of 2.5% and were boiled for 5 min. Low molecular mass calibration standards (16.9, 14.4, 10.7, 8.1, 6.2, and 2.5 kDa, from Pharmacia) were run alongside the sample.

The gel was stained using a silver staining technique per manufacturer's instructions with minor modifications. Briefly, gels were fixed in 25% glutaraldehyde for 10 min, washed twice with water for 5 min, then stained in a 0.5% silver nitrate solution for 45 min. After two washes with water, the gels were developed in a 2.5% sodium carbonate buffer containing 0.015% formaldehyde for approximately 12 min. Gels were soaked in a bath of 10% aqueous acetic acid containing 10% glycerol for 30 min to preserve.

Light scattering

Buffers were filtered through a 0.22-μm filter and degassed prior to use. Solutions were passed through a 0.45-μm Millipore filter to remove dust. The concentration was re-examined by absorbance, and pH of the solution was measured. The peptide solution was then transferred to a precleaned, dust-free cuvette. The cuvette was placed in a sample holder, which contained decahydronaphthalene (Aldrich Chemical Co., Milwaukee, WI) as a refractive index matching fluid. The sample was maintained at 25 ± 0.1°C using a temperature-controlled circulating water bath. Experiments were performed using the Malvern (Spring Lane, United Kingdom) 4700c particle analyzer with a 128-channel autocorrelator and a Lexel (Fremont, CA) Model 95–2 argon-ion laser equipped with an etalon and operated at a power of 75–200 mW and at a wavelength of 488 nm. In order to reduce stray light, the equipment was enclosed in a black box.

Classical light scattering (CLS) experiments were performed essentially as described previously (Tomski and Murphy, 1992). Briefly, the scattered light intensity of the sample was collected for 20 s at 17 different angles between 20° and 140°. Each measurement was repeated ten times, and then averaged. The scattered light intensity of the buffer was then measured at the same conditions and subtracted from the sample intensity. The results were normalized with respect to intensity data from spectrophotometric grade toluene (Aldrich) to obtain the Rayleigh ratio of the sample $R_s(q)$.For dilute polydisperse solutions,

$$R_s(q) = \sum_i K_i c_i M_i P_i(q)[1 - 2B_i c_i M_i P_i(q)] \quad (1)$$

where the subscript i is a counter for each macromolecular species, $K = 4\pi^2 n^2 (dn/dc)^2 / N_A \lambda_o^4$, n is the refractive index of the solvent, dn/dc is the refractive index increment, N_A is Avogadro's number, λ_o is the laser wavelength in vacuo, c is concentration in g/ml, M is molecular weight, B is the second virial coefficient, and $P(q)$ is the particle structure factor which accounts for intramolecular interference (Geiduschek and Holtzer, 1958).

For our system, K is assumed to be independent of state of aggregation. At low angles (low q, where $q = (4\pi n/\lambda_0)\sin(\theta/2)$ is the scattering vector) and low concentration, Eq. 1 then simplifies to

$$\frac{Kc}{R_s(q)} = \frac{1}{\langle M \rangle_{w,app}} \left(1 + \frac{1}{3} q^2 \langle R_g^2 \rangle_z \right), \quad (2)$$

where $\langle M\rangle_{w,app}$ is the apparent weight-averaged molecular weight and $\langle R_g^2\rangle_z$ is the light-scattering-averaged squared radius of gyration. For rods, $\langle R_g^2\rangle_z^{1/2}$ corresponds to the radius of gyration of a rod of molecular weight slightly greater than the z-average molecular weight and can be related to the rod length as

$$\langle L\rangle_z = 12\langle R_g^2\rangle_z^{1/2}. \tag{3}$$

A plot of $Kc/R_s(q)$ vs. q^2 yields an intercept corresponding to the inverse of $\langle M\rangle_{w,app}$ and a slope from which $\langle R_g^2\rangle_z^{1/2}$ can be calculated.

If the particles in solution are rigid rods which are heterogeneous in diameter, then at low concentrations and large scattering angles ($qL \gg 1$) Eq. 1 simplifies to (Geiduschek and Holtzer, 1958)

$$\frac{Kc}{R_s(q)} = \frac{2}{\pi^2}\frac{\langle M/L^2\rangle_w}{\langle M/L\rangle_w^2} + \frac{q}{\pi\langle M/L\rangle_w}. \tag{4}$$

A plot of $Kc/R_s(q)$ vs. q yields a straight line. The inverse of the intercept is proportional to an average molecular weight which for rods of homogeneous diameter reduces to the number-average molecular weight $\langle M\rangle_n$ and which we will refer to as $\langle M\rangle_{n,app}$. The slope is proportional to a weight-average linear molecular density, which can be converted to a weight-averaged rod diameter $\langle d\rangle_w$ using the estimated hydrated specific volume V_h of β(1–28) of 1.17 ml/g (Kuntz and Kauzmann, 1974; Cohn and Edsall, 1943) and the equation:

$$\left\langle\frac{M}{L}\right\rangle_w = \frac{\pi\langle d\rangle_w^2}{4}\frac{N_A}{V_h}. \tag{5}$$

For determination of dn/dc, solutions of peptide were made up at known concentrations and the refractive index of the solution was measured using a Milton-Roy (Rochester, NY) Abbe-3L refractometer. The refractive index increment was determined to be 0.24 ± 0.03 ml/g. Refractometer calibration was checked using aqueous solutions of NaCl (Huglin, 1972).

For quasielastic light scattering (QLS) experiments, the scattered light intensity at five angles (30°, 45°, 70°, 90°, and 120°) was collected and converted to the normalized first-order electric field autocorrelation function $g^{(1)}(\tau)$. Data were collected 20 times for 30-s duration each time and then averaged. Data were analyzed using the method of cumulants (Koppel, 1972) where

$$\ln|g^{(1)}(\tau)| = -\langle\Gamma\rangle\tau + \frac{1}{2!}\mu_2\tau^2 - \frac{1}{3!}\mu_3\tau^3 + \cdots \tag{6}$$

$\langle\Gamma\rangle$ is the initial decay rate and τ is the decay time. The apparent translational diffusion coefficient $\langle D\rangle_{z,app}$ was calculated from

$$\langle D\rangle_{z,app} = \frac{\langle\Gamma\rangle}{q^2}. \tag{7}$$

The notation indicates that the diffusion coefficient is z-averaged and is thus weighted toward larger particles. This is an apparent diffusion coefficient because the influence of particle shape factor, internal motions of the particle, or particle-particle interactions are not included. $\langle D\rangle_{z,app}$ was converted to an apparent hydrodynamic radius $\langle R_h\rangle_{z,app}$ using the Stokes-Einstein equation:

$$\langle R_h\rangle_{z,app} = \frac{k_BT}{6\pi\eta\langle D\rangle_{z,app}} \tag{8}$$

where k_B is the Boltzmann constant and η is the solvent viscosity. Alternatively, data were fit to a diffusion coefficient distribution using the program CONTIN (Provencher, 1982). Note that the inverse of the hydrodynamic radius is z-averaged, and then inverted, to obtain $\langle R_h\rangle_{z,app}$.

Theoretical calculations of $\langle\Gamma\rangle/q^2$ vs. q^2 for rods of various lengths and diameters were carried out as follows. Maeda and Fujime (1984) derived the following expression for a dilute solution of monodisperse rigid rods

$$\frac{\langle\Gamma\rangle}{q^2} = D + \frac{L^2}{12}\Theta f_1 + (D_3 - D_1)\left(f_2 - \frac{1}{3}\right) \tag{9}$$

where D_1 and D_3 are the diffusivities perpendicular and parallel to the rod length, respectively, and $D = (2D_1 + D_3)/3$. This equation incorporates the effects of rotation and anisotropic translation on the diffusive motion detected in QLS experiments. The factors f_1 and f_2 are complex functions of qL and were calculated from the numerical values given by Maeda and Fujime (1984). The following limits apply

$$\frac{\langle\Gamma\rangle}{q^2} = D \qquad (qL \ll 1)$$

$$\frac{\langle\Gamma\rangle}{q^2} = D - \frac{1}{3}(D_3 - D_1) + \frac{L^2}{12}\Theta \qquad (qL \gg 1). \tag{10}$$

The Broersma equations (Russo et al., 1984) were used to calculate the translational diffusion coefficient D and the rotational diffusion coefficient Θ as a function of rod length and diameter. Specifically

$$D = \frac{k_BT}{3\pi\eta L}\left[\delta - \frac{1}{2}(\gamma_1 + \gamma_3)\right]$$

$$\Theta = \frac{3k_BT}{\pi\eta L^3}(\delta - \epsilon)$$

$$\delta = \ln\left(\frac{2L}{d}\right) \tag{11}$$

$$\gamma_1 = 0.19 - 4.2(\delta^{-1} - 0.39)^2$$

$$\gamma_3 = 1.27 - 7.4(\delta^{-1} - 0.34)^2$$

$$\epsilon = 1.45 - 7.5(\delta^{-1} - 0.27)^2.$$

The long-rod limit $D_3 = 2D_1$ was used to calculate these diffusivities from the Broersma relations.

Electron microscopy

A drop of the peptide solution was placed on a Pioloform-coated 300-mesh electron microscope copper grid. After blotting, a drop of 1% ammonium molybdate was placed on the grid while it was held with fine forceps. The grid was blotted on filter paper and allowed to dry before observing the specimen in a JEOL (Peabody, MA) 100 CX Electron Microscope at 60 kV.

RESULTS

Secondary structure

The circular dichroism spectra of β(1–28) is shown in Fig. 1. Analysis of the spectra indicates that the peptide exists as 100% unordered conformation at these conditions.

Oligomerization

Peptide solutions were analyzed by size exclusion HPLC repeatedly over a period of 7–10 days. A representative chromatogram is shown in Fig. 2. Analysis of the chromatograms indicated the presence of one major peak, with an elution time corresponding to a molecular weight of approximately 13,000 (tetramer), and a smaller peak with an elution time corresponding to a molecular weight of a monomer. Chromatograms were not significantly different at any of the three concentrations tested (0.2, 0.5, and 1.0 mg/ml), were not affected by the presence or absence of NaCl in the injected sample, and did not change substantially over the test period (30 min to 7–10 days after sample preparation). The percent monomer (based on the peak area for monomer relative to the

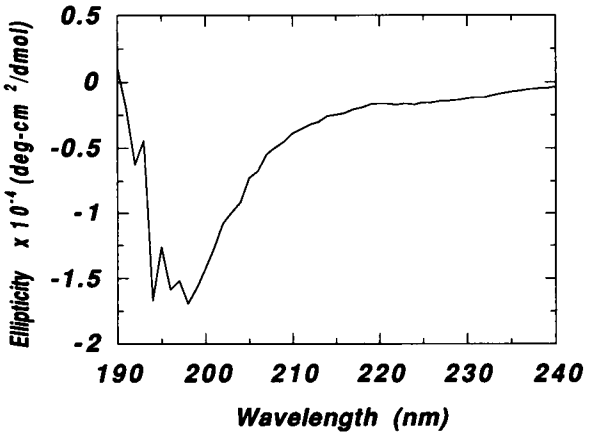

FIGURE 1 Circular dichroism spectra for 0.2 mg/ml β(1–28) in 0.02 M phosphate buffer, pH 7.4. The sample was analyzed 3 h after sample preparation.

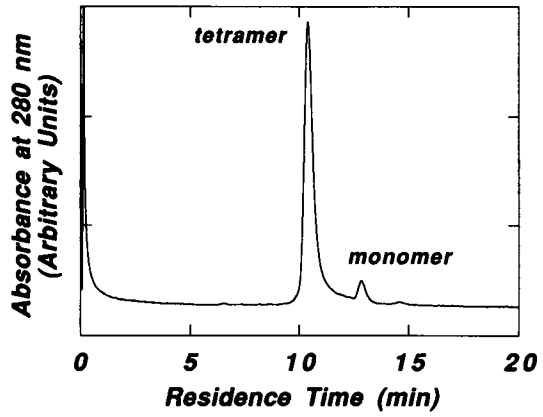

FIGURE 2 Representative size-exclusion HPLC chromatogram of β(1–28). The mobile phase is PBSA.

total peak area) was relatively constant at ~5 ± 2% independent of concentration, salt content, or time after sample preparation. Total peak area did not change significantly with time after sample preparation.

The presence of peptide oligomers was further investigated by SDS-PAGE. Representative results are shown in Fig. 3. Two bands were detected: one corresponding to a molecular mass of 4 kDa and a broader band corresponding to a molecular mass of 11–13 kDa. A small band was also detected which was excluded from the gel. Peptide solutions were incubated from 1 h to 13 days prior to analysis. The presence and distribution of bands did not change noticeably with concentration or with aging of the sample.

In order to determine if the apparent tetramer bound Congo red, either Congo red dye alone or a Congo red-peptide mixture was injected into the column, with peak detection set at 485 nm. There was only a single peak in both cases at identical residence times, corresponding to the elution time of the free dye, indicating that the dye did not co-elute with the tetramer.

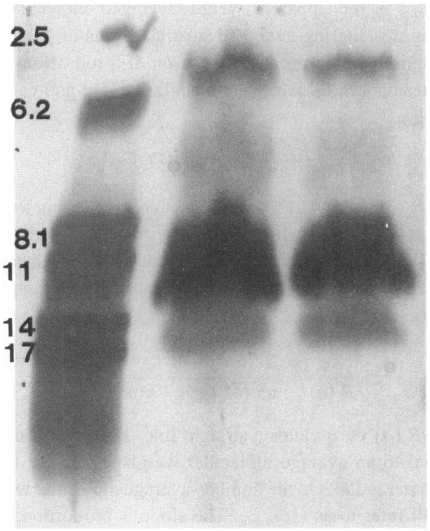

FIGURE 3 Representative SDS-PAGE gel. Lane 1, molecular weight standards; lane 2, 1 mg/ml β(1–28); lane 3, 0.5 mg/ml β(1–28). The solutions shown here were aged 19 days prior to application to the gel. Shorter aging times did not materially alter the appearance of the gels. Molecular masses of the protein markers (in kilodaltons) are shown to the left of lane 1.

Cross-β-pleated sheet structure

Congo red absorbance spectroscopy and ThT fluorescence spectroscopy were used to probe for the presence of cross-β-pleated sheet structure, a defining characteristic of amyloid fibrils. Difference spectra, shown in Fig. 4, indicated that the degree of Congo red binding increased significantly as the concentration increased from 0.2 to 0.5 mg/ml. Consistent with the Congo red results, ThT fluorescence intensity increased dramatically from 0.2 to 0.5 mg/ml (Fig. 5). There was no significant difference between samples prepared at low and physiological ionic strength.

In these experiments, Congo red absorbance spectra were taken after incubating the peptide with the dye for 1 h,

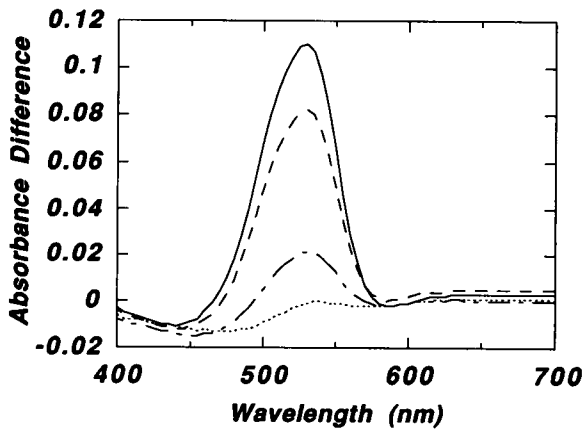

FIGURE 4 Absorbance difference spectra for 7 μM Congo red in the presence of varying concentrations of β(1–28) in PBSA. Samples were incubated for 1 h at room temperature prior to analysis. Dotted line, 0.2 mg/ml; dash-dot line, 0.3 mg/ml; dash line, 0.4 mg/ml; solid line, 0.5 mg/ml.

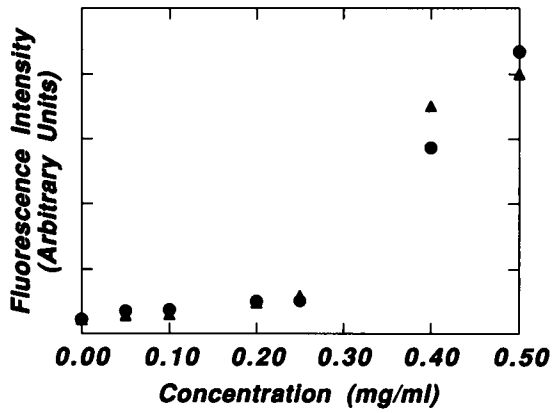

FIGURE 5 Fluorescence intensity of 1 μM ThT as a function of β(1–28) concentration. Solid circles show data taken in 0.01 M phosphate buffer (pH 7.4), and solid triangles show data taken in PBSA. Excitation was at 450 nm and emission at 482 nm. Peptide solutions were incubated for 24 h prior to addition of ThT. Similar results were obtained for solutions incubated for 1 h prior to ThT addition.

whereas ThT fluorescence intensity measurements were taken by incubating the peptide in the absence of the dye for 1 or 24 h, then adding the dye and rapidly taking the measurement. No difference in the concentration threshold was observed for these two different methods.

Fibril formation kinetics

Several β(1–28) samples were subjected to light scattering and electron microscopy analysis. Sample A was prepared by dissolving 1 mg of lyophilized peptide in 1 ml of 0.01 M phosphate buffer (final pH 7.3). Total intensity measurements were taken over time and analyzed using Eqs. 2 and 4. Representative data taken at 168 h after sample preparation are shown in Fig. 6. Plots of $Kc/R_s(q)$ vs. q^2 curved downward (Fig. 6 *A*), whereas plots of $Kc/R_s(q)$ vs. q were linear (Fig. 6 *B*). Both of these results are consistent with a rodlike particle structure. $\langle M\rangle_{w,app}$ was calculated from the limiting slope as q^2 approaches zero, per Eq. 2. Results are shown in Fig. 7 and Table 1. $\langle M\rangle_{w,app}$ was 600 ± 90 kDa (corresponding to a weight-average of 185 monomers) after 8 h and increased by a factor of four over the next 120 h. At this point there was a sharp increase in the rate of growth. After 240 h, the solution was diluted in half, to a peptide concentration of 0.5 mg/ml, and data collection was continued for 6 more days. A significant decrease in size occurred upon dilution, as shown in Table 1 and Fig. 7.

$\langle M\rangle_{n,app}$ was calculated from the plot of $Kc/R_s(q)$ vs. q per Eq. 4. Results are shown in Table 1. $\langle M\rangle_{n,app}$ was 140 ± 10 kDa after 8 h, corresponding to 43 monomers per aggregate on a number-averaged basis. $\langle M\rangle_{n,app}$ increased with time, concomitant with the increase in $\langle M\rangle_{w,app}$, although the rate of increase was not nearly as rapid.

$\langle R_g^2\rangle_z^{1/2}$ and $\langle M/L\rangle_w$ were determined from the slopes of the data, plotted per Eqs. 2 and 4, respectively. Results are shown

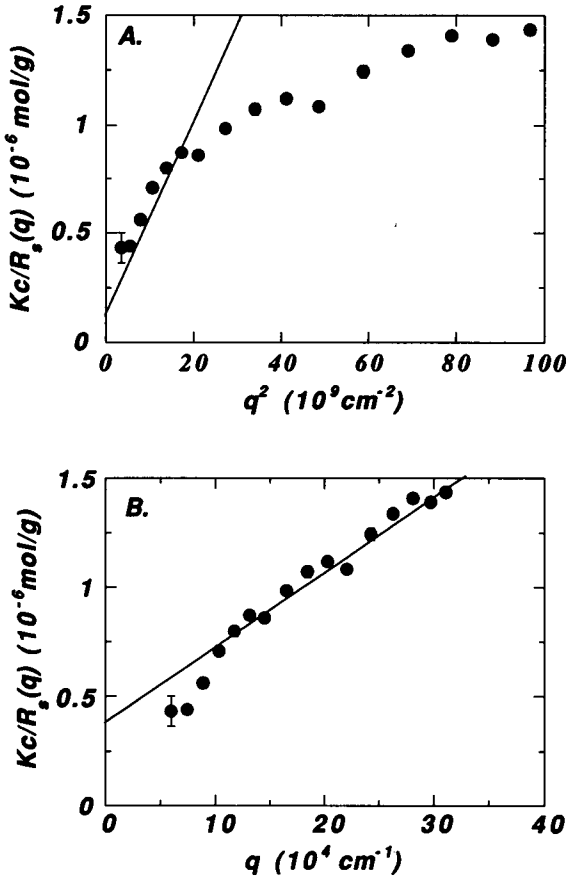

FIGURE 6 $Kc/R_s(q)$ versus scattering vector for 1 mg/ml β(1–28) in 0.01 M phosphate buffer (sample A). Data were collected 168 h after sample preparation. Straight line shows linear fit to data using (*A*) Eq. 2 or (*B*) Eq. 4.

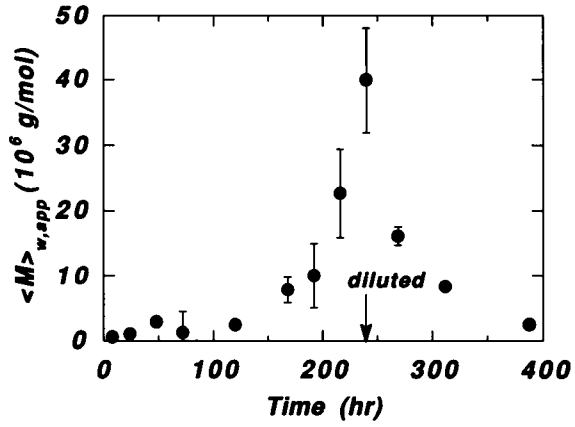

FIGURE 7 $\langle M\rangle_{w,app}$ versus time for 1 mg/ml β(1–28) in 0.01 M phosphate buffer (sample A). Sample was diluted in half 240 h after preparation.

in Table 1. $\langle L\rangle_z$ (Eq. 3) varied from approximately 900–1400 nm and $\langle d\rangle_w$ (Eq. 5) increased from 1.4 to 8.6 nm over this time period. $\langle R_g^2\rangle_z^{1/2}$ fluctuated considerably but did not change significantly during the first 240 h. An increase in $\langle M/L\rangle_w$ occurred with time (Table 1). Both $\langle R_g^2\rangle_z^{1/2}$ and $\langle M/L\rangle_w$ decreased upon dilution.

TABLE 1 Analysis of classical light scattering data: sample A

Time	$\langle M\rangle_n$	$\langle M/L\rangle_w$	$\langle M\rangle_w$	$\langle R_g^2\rangle_z^{1/2}$	$\langle R_h\rangle_z$
hr	10^3 g/mol	10^9 g/mol-cm	10^3 g/mol	10^{-7} cm	10^{-7} cm
1	ND	ND	ND	ND	42
4	ND	ND	ND	ND	60
8	136 ± 9	7.9 ± 0.8	602 ± 87	267 ± 24	107
24	176 ± 4	16.1 ± 0.8	1070 ± 3	265 ± 2	136
48	248 ± 17	16.1 ± 0.8	2890 ± 710	447 ± 60	190
72	327 ± 200	29.4 ± 3.2	NR‡	NR	203
120	NR	31.6 ± 0.8	2420 ± 387	210 ± 30	225
168	657 ± 23	85.2 ± 0.8	7810 ± 2000	350 ± 50	327
192	762 ± 34	108.9 ± 0.8	10000 ± 5000	360 ± 110	416
216	2780 ± 420	126.3 ± 1.6	22700 ± 6710	430 ± 70	588
240	8110 ± 1650	297.9 ± 1.6	40000 ± 8100	360 ± 40	659
		Sample was diluted to 0.5 mg/ml			
269	1690 ± 41	264.3 ± 0.8	16200 ± 1370	280 ± 10	406
312	1930 ± 88	203.0 ± 0.8	8260 ± 552	190 ± 10	344
388	579 ± 13	121.8 ± 0.8	2480 ± 114	128 ± 7	ND

* ND, not determined.
‡ NR, not reported.

QLS measurements were taken for the same sample over the same time period. Data taken at 90° were analyzed for apparent diffusion coefficients, and this was converted to an apparent hydrodynamic radius. Results are shown in Fig. 8. $\langle R_h\rangle_{z,app}$ increased rapidly, then stabilized at approximately 250 nm from about 50–150 h, then increased rapidly again. After 240 h, data collection was stopped because of the appearance of a damped oscillatory autocorrelation function. Upon dilution to 0.5 mg/ml, measurements could again be taken, and $\langle R_h\rangle_{z,app}$ decreased to about 300 nm.

QLS data were further analyzed as a function of angle. Representative plots of $\langle\Gamma\rangle/q^2$ vs. q^2 are shown in Fig. 9. The data are compared to theoretical calculations (Eqs. 9–11) for rods of 5-nm hydrodynamic diameter and lengths of 500–5000 nm. The data suggest that at early times (~1 h), the fibrils have already reached lengths of approximately 500 nm or more. With increasing time, the apparent length of the fibrils increased rapidly. Diffusivities measured at 24 h are consistent with fibril lengths reaching 2000–5000 nm.

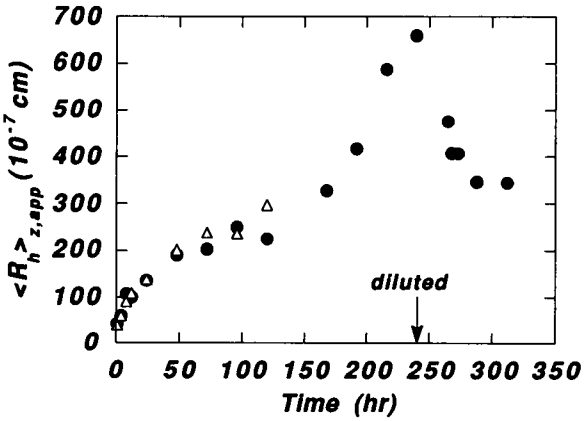

FIGURE 8 $\langle R_h\rangle_{z,app}$ versus time for 1 mg/ml β(1–28) in 0.01 M phosphate buffer (sample A). Sample was diluted in half 240 h after preparation. Solid circles show results from 90° QLS data using cumulants analysis; open triangles show results based on CONTIN analysis. Error bars are approximately the size of the symbols. Fitting of data at longer times was attempted with CONTIN; however, nonrandom residuals were obtained.

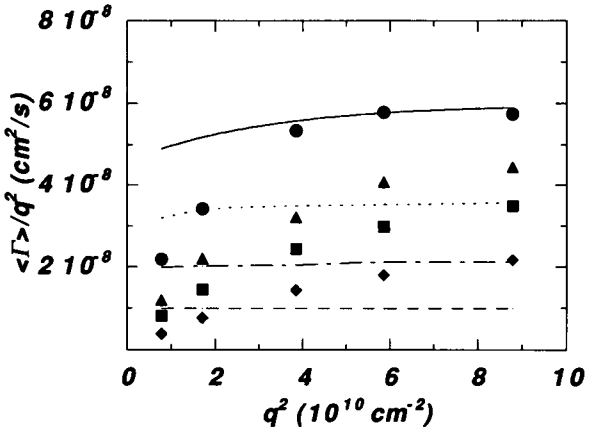

FIGURE 9 $\langle\Gamma\rangle/q^2$ vs. q^2 for 1 mg/ml β(1–28) in 0.01 M phosphate buffer (sample A) 1 h (*solid circles*), 4 h (*solid triangles*), 8 h (*solid squares*), and 24 h (*solid diamonds*) after sample preparation. Lines represent calculations based on Eqs. 9 and 11: d = 5 nm, L = 500 nm (*solid line*); d = 5 nm, L = 1000 nm (*dotted line*); d = 5 nm, L = 2000 nm (*dot-dash line*); d = 5 nm, L = 5000 nm (*dash line*).

Electron micrographs of sample A were taken approximately 21 and 45 h after initial preparation. Additionally, the sample which was studied extensively by CLS and QLS was examined three months after preparation. At 21 h, only a few rodlike fibrils were evident (Fig. 10 *A*). The fibrils showed a definite twist, and had diameters of roughly 10 nm and lengths of roughly 500–1000 nm. The fibril dimensions seen on micrographs are similar to those reported by others (Castano et al., 1986; Kirschner et al., 1987; Fraser et al., 1991) and are consistent with naturally occurring amyloid fibril dimensions. After 45 h (Fig. 10 *B*), the number density of fibrils had increased substantially. Rod diameter and fibril morphology were similar; lengths were difficult to determine precisely but were greater than 2000 nm in some cases. After

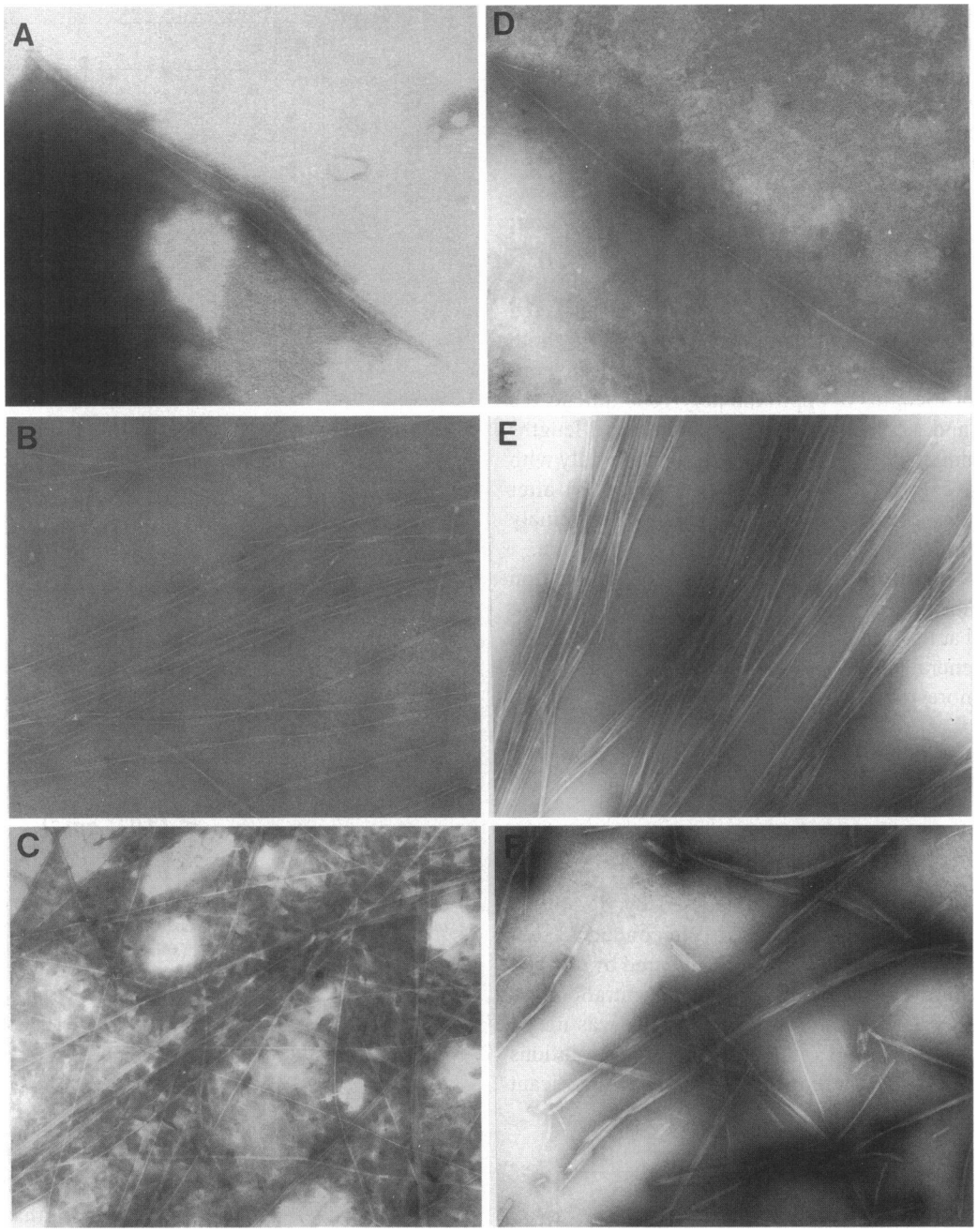

FIGURE 10 Electron micrographs. (*A*) 1 mg/ml β(1–28) in 0.01 M phosphate buffer (sample A), 21 h after sample preparation, 90,000 × magnification. (*B*) Same as *A*, except 45 h after sample preparation, 72,500 × magnification. (*C*) Diluted sample A, 3 months after sample preparation, 47,500 × magnification. (*D*) 1 mg/ml β(1–28) in PBSA (sample D), 3 h after sample preparation, 72,500 × magnification. (*E*) Same as *D*, except taken 7 weeks after sample preparation, 47,500 × magnification. (*F*) 1 mg/ml β(1–28) at pH 4.4, 35,000 × magnification.

3 months, an extended entanglement of fibrils of similar diameter but indeterminant lengths had formed (Fig. 10 *C*).

An attempt was made to measure the aggregation process on a sample prepared in the same 0.01 M phosphate buffer at 0.5 mg/ml initial concentration, but after 7 days no measurable scattering signal was detected.

Sample B was prepared by dissolving 1 mg of lyophilized β(1–28) in 0.5 ml of 0.01 M phosphate buffer, vortexing briefly, then diluting in 0.5 ml of phosphate buffered saline to produce a final NaCl concentration of 0.14 M and a final pH of 7.3. QLS data were obtained for this sample and analyzed. Over the first 24 h, $\langle R_h \rangle_{z,app}$ and $\langle \Gamma \rangle / q^2$ were quite similar to that for sample A (data not shown). However, after 24 h the sample containing NaCl increased sharply in size and the autocorrelation function became oscillatory.

Samples C and D were prepared by dissolving 0.5 and 1.0 mg of lyophilized peptide, respectively, into PBSA. Final pH was 7.5 for sample C and 7.3 for sample D. The aggregation

rate was too rapid to collect CLS measurements. $\langle R_h \rangle_{z,app}$ as a function of time was determined by analysis of QLS data taken at 90° (Fig. 11). There was a rapid increase in the particle size, with the rate approximately tripling with a doubling in the concentration. The experiments were stopped due to the onset of an oscillatory autocorrelation function after 8 h for 1 mg/ml and after 24 h for 0.5 mg/ml. Attempts were made to collect data at 0.2 mg/ml in the same buffer; however even after 9 days incubation there was no detectable signal.

Multiangle QLS data for samples C and D were analyzed and compared to theoretical calculations (Fig. 12). For both samples C and D, diffusivities measured after 1 h were consistent with fibril lengths of approximately 1000 nm. At 2 h for sample D and 4 h for sample C, apparent fibril lengths reached 5000 nm or more. Diffusivities dropped rapidly with time, reaching extremely low values ($\sim 10^{-9}$ cm^2/s) after 8–12 h. These low diffusivities are consistent with extremely long fibrils, approaching apparent lengths of 50,000 nm.

Sample D was analyzed 3 h after preparation by electron microscopy. Fibril morphology and diameter were similar to those prepared at low ionic strength. At this early time, fibril density was generally low, and lengths ranged from 600 to 3000 nm or more (Fig. 10 *D*). The same sample was inspected seven weeks later. A substantial amount of side-by-side alignment of fibrils into large bundles had occurred by this time (Fig. 10 *E*).

Effect of sample preparation method

The above experiments were all conducted by dissolving lyophilized peptide directly into buffer. We conducted several experiments in which samples were prepared by dilution from a stock solution at 10 mg/ml peptide concentration prepared in 0.1% TFA. ThT fluorescence intensity was measured for samples prepared from 0.1% TFA stock solutions and diluted into PBSA. These samples showed a significant increase in ThT fluorescence comparable to that shown in Fig. 5, indicating the presence of cross-β-pleated sheet structure (data not shown). A sample was prepared by diluting the 0.1% TFA stock solution into PBSA with a final peptide concentration of 1 mg/ml and a final pH of 6.8. QLS measurements taken on this sample indicated that the rate of increase in size was similar to that for an equivalent sample (sample D) prepared directly from lyophilized peptide (Fig. 11). However, the intensity of scattered light was considerably diminished relative to that for sample D, indicating a lower fibril concentration. Electron microscopy analysis confirmed that there were far fewer fibrils present when the peptide was prepared by dissolution first in TFA, although the fibril morphology was similar (data not shown). Interestingly, samples prepared by dissolving the stock solution first in phosphate buffer containing no saline, then adding saline to a final concentration of 0.14 M NaCl, showed no detectable aggregation.

We attempted to obtain light scattering results on a sample prepared at 0.5 mg/ml and low pH (pH 4.6). The sample

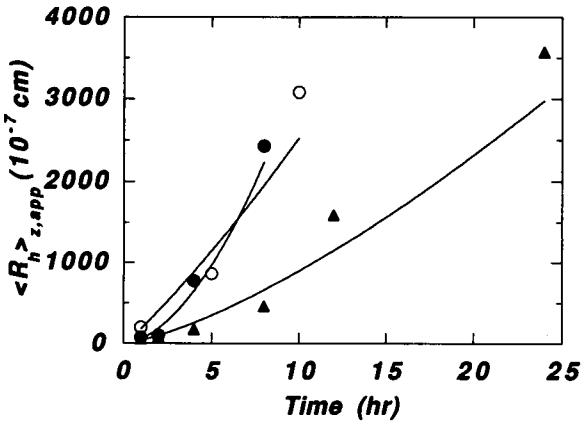

FIGURE 11 $\langle R_h \rangle_{z,app}$ versus time for β(1–28) in PBSA. QLS data were taken at 90° scattering angle and analyzed by the method of cumulants. Solid circles, 1 mg/ml (sample D); solid triangles, 0.5 mg/ml (sample C); open circles, 1 mg/ml in PBSA (final concentration), prepared from stock solution of 10 mg/ml in 0.1% TFA.

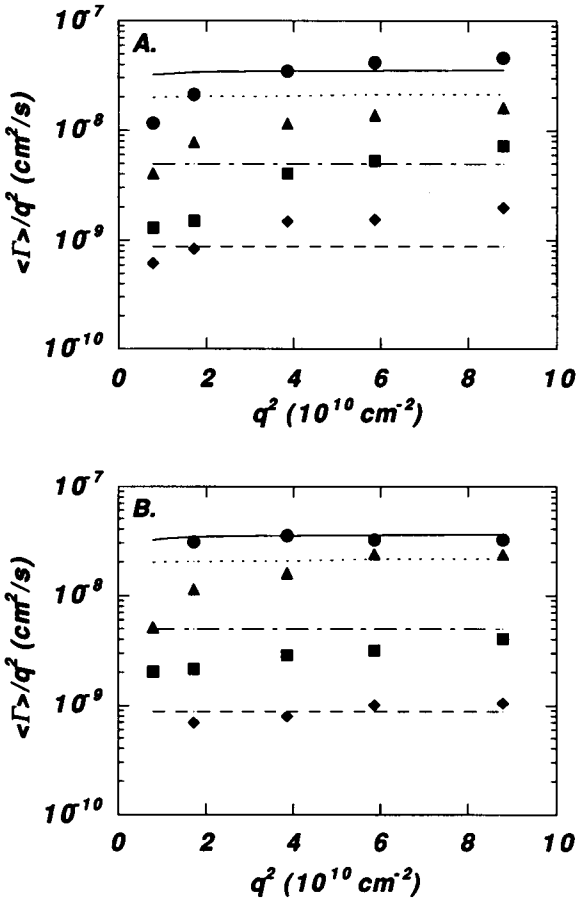

FIGURE 12 (*A*) $\langle \Gamma \rangle / q^2$ vs. q^2 for 0.5 mg/ml β(1–28) in PBSA (sample C) 1 h (*solid circles*), 4 h (*solid triangles*), 8 h (*solid squares*), and 12 h (*solid diamonds*) after sample preparation. (*B*) $\langle \Gamma \rangle / q^2$ vs. q^2 for 1 mg/ml β(1–28) in PBSA (sample D) 1 h (*solid circles*), 2 h (*solid triangles*), 4 h (*solid squares*), and 8 h (*solid diamonds*) after sample preparation. For both graphs, lines represent calculations based on Eqs. 9 and 11: d = 5 nm, L = 1000 nm (*solid line*); d = 5 nm, L = 2000 nm (*dotted line*); d = 10 nm, L = 10,000 nm (*dot-dash line*); d = 100 nm, L = 50,000 nm (*dash line*).

rapidly became turbid and a damped oscillatory autocorrelation function was observed. After filtration through a 0.45-μM filter, no signal was obtained from the supernatant. Electron micrographs of a sample prepared in this manner showed more heterogeneity in rod diameter, more heterogeneity in length, and less lateral aggregation than the sample prepared at neutral pH (Fig. 10 *F*).

DISCUSSION

β-A/4 has been proposed to be a causative agent in the onset or development of neuronal disorders in Alzheimer's disease. Toxicity studies with synthetic versions of β-A/4 have led to inconclusive results. Given recent data that the aggregation state of the peptide may influence the toxicity, a more detailed examination of fibril formation is warranted. We have set out to combine a variety of physicochemical techniques to probe the self-assembly process of synthetic peptides homologous to β-A/4. Here, we report our results for β(1–28), which is a useful model peptide to study in comparison to the longer peptides, for investigating the role of the extracellular domain in self-assembly and fibril formation.

CD results show that β(1–28) does not adopt a regular structure at 0.2 mg/ml in 0.02 M phosphate buffer. These results are consistent with those reported by others for β(1–28) in phosphate buffer at pH 7.3 (Barrow and Zagorski, 1991) or in water at pH 2.8 (Barrow et al., 1992). In contrast, Hilbich and coworkers reported that β(1–27) contained 14% β-sheet, 33% β-turn, 7% α-helix, and 46% random coil under similar conditions to ours (Hilbich et al., 1991a). Fraser et al. (1991a) reported Fourier transform infrared experiments which indicated that β(1–28) at 5–20 mg/ml contained 70–80% β-sheet at pH 4–7.The differences may be due to a concentration dependence of formation of intermolecular β-sheet structures.

Despite the lack of a detectable regular structure in solution, β(1–28) self-assembles into small oligomers. Size-exclusion HPLC analysis indicated that the peptide eluted at molecular weights corresponding to tetrameric and monomeric species, with the tetramer dominating. Fibrils were not detected eluting from the column, probably because they were trapped by the guard column. Molecular weight determination by size exclusion chromatography can be uncertain due to variable elution times caused by alternate conformations (e.g., compact versus extended structures) or by weak electrostatic interactions with the column. However, SDS-PAGE experiments also showed that the major species migrated with molecular weight close to that of a tetramer. Others have also reported the presence of monomer and tetramer for β(1–28), although the degree of tetramerization was much less (Barrow et al., 1992).

Neither the total peak area nor the percent tetramer changed significantly over a test period of 7–9 days. The percent tetramer did not change substantially with concentration, or in the presence or absence of NaCl in the sample solution. There does not appear to be a rapid interconversion between the tetramer and monomer (i.e., over the time course of the HPLC experiment), as evidenced by fairly sharp and symmetric peaks. Thus, the tetramer appears to be a very stable noncovalent oligomer of β(1–28). It is surprising that a stable oligomer is formed in the absence of a regular secondary structure. Since the CD spectra were taken in the absence of NaCl (due to interference from its absorbance in the UV) and the mobile phase in the HPLC experiments contained NaCl (to reduce electrostatic interactions between the peptide and the column), it is conceivable that the addition of NaCl leads to rapid formation of secondary structure with subsequent rapid assembly into tetramers. However, if this were true, one might expect chromatograms for samples prepared with and without NaCl to differ somewhat due to the time delay for diffusion of NaCl from the mobile phase into the sample, formation of secondary structure, and self-assembly. This was not observed. Alternatively, the absence of regular secondary structural features in the CD spectra does not necessarily mean that the peptide is in a completely random configuration (Woody, 1985).

The tetramer does not appear to bind ThT or Congo red. This was shown in two ways: first, Congo red coinjected with peptide eluted on HPLC as free dye. Second, peptide concentrations of 0.2 mg/ml contained significant amounts of tetramer but did not bind Congo red or ThT. However, the cross-β structure characteristic of amyloid fibrils is present in these samples at concentrations of ~0.3 mg/ml or greater. We suggest that ThT and Congo red bind only to higher-order aggregates, which we tentatively term protofibrils. It is conceivable that these protofibrils correspond in some way to the subunits reported by others in electron micrograph and x-ray diffraction studies (Fraser et al., 1991b; Inouye et al., 1993). Salt concentration is not a significant factor in determining the minimum concentration required for the formation of protofibrils.

Fibril formation kinetics of 1 mg/ml β(1–28) solution in 0.01 M phosphate (sample *A*) were studied in detail by light scattering and electron microscopy. Analysis of CLS data is not straightforward for this system. Polydispersity, intraparticle scattering interference, and intermolecular interactions influence the scattering intensity. Conventional Zimm plots are not appropriate because aggregation is a function of concentration. The accuracy of the values of $\langle M\rangle_w$ and $\langle R_g^2\rangle_z^{1/2}$ depend on the validity of the assumptions used to derive Eq. 2. The assumption that $P(q)^{-1} = 1 + q^2\langle R_g^2\rangle_z/3$ is valid for rods to $q^2\langle R_g^2\rangle_z \sim 4$ (Geiduschek and Holtzer, 1958). Due to the size of the aggregates formed in our work, this approximation is applicable only for scattering angles of ~35° or less. Nevertheless, in order to have a reasonable number of data points to determine $\langle R_g^2\rangle_z$, scattering intensities to ~45° were used in data fitting. A more difficult problem arises because no correction for the second virial coefficient B was made. Assuming only hard-core repulsive interactions, the second virial coefficient can be calculated from

$$B = \frac{\pi N_A d}{4}\left(\frac{L}{M}\right)^2, \qquad (12)$$

which is appropriate for long rods (Tracy and Pecora, 1992). Using the values of $\langle M/L\rangle_w$ from Table 1 to calculate B from Eq. 12, and applying this calculation to Eq. 1, leads to estimates that $\langle M\rangle_w$ may be 1.1 to ~4 times larger than $\langle M\rangle_{w,app}$ in some cases. This may be an overestimate of the correction factor required, due to complications such as the broad polydispersity and fibril flexibility. Attractive or repulsive solute-solute interactions may further alter the numerical value of B (Nicolai and Mandel, 1989a), but it is difficult to calculate the magnitude of these effects. When $\langle M\rangle_w$ is calculated directly from $\langle M/L\rangle_w$ and L, results are reasonably consistent with the values of $\langle M\rangle_{w,app}$ reported in Table 1. Finally, it should be noted that these peptide solutions are very polydisperse, and that the values reported reflect molecular properties averaged over all species in solution. For example, a solution with $\langle M\rangle_w = 10^6$ could consist of 90 wt% tetramer ($M = 1.3 \times 10^4$) and 10% long fibrils ($M = 10^7$). $\langle R_g^2\rangle_z$ is heavily weighted toward the larger particles and more likely reflects primarily properties of the fibrils.

From CLS data at 24 h, the average fibril length was calculated to be ~900 nm. This is consistent with the fibril lengths of 500–1000 nm seen on electron micrographs at 21 h. In contrast, multiangle analysis of QLS data and comparison to theoretical calculations of $\langle\Gamma\rangle/q^2$ for long rods show that the measured diffusivities at 24 h are consistent with fibril lengths of 2000–5000 nm. Moderate changes in the assumed rod diameter (factor of 2–3) do not result in substantially different values for $\langle\Gamma\rangle/q^2$.

Consideration of the interpretation of QLS data for long thin rods is necessary to explain this apparent discrepancy. The theoretical expressions (Eqs. 9 and 11) ignore the influence of polydispersity, rod flexibility, and fibril-fibril interactions. The angular dependence seen in the data but not in the theoretical calculations (Fig. 9) is most likely the result of polydispersity. Rod flexibility would increase the diffusivity above that for a stiff rod of the same contour length, which does not explain the discrepancy in fibril length between QLS and EM data. Thermodynamic and hydrodynamic interactions, which become increasingly important as the concentration increases, influence the effective diffusivity measured in QLS experiments. Theoretical and experimental work show that repulsive electrostatic interactions increase the diffusive motion measured by QLS relative to uncharged rods (Weyerich et al., 1990; Nicolai and Mandel, 1989b), which again does not explain the discrepancy between QLS and EM data.

The most likely explanations for the anomalously low diffusivities are the formation of loose fibril aggregates and the onset of caging, in which the rotational and sideways translational diffusion are reduced due to the effect of interactions with neighboring rods. The effect of caging is estimated to become measurable at values of $NL^3 > 35$–50 (Keep and Pecora, 1988), where N is the number density of rods. For fibrils with lengths of ~1000 nm, and molecular weights of $\sim 10^7$, the corresponding concentration of fibrils at which caging might be observed is ~0.5–0.8 mg/ml, compared to a total peptide concentration of 1 mg/ml. Caging effects can influence dynamic properties such as diffusion without altering static properties such as radius of gyration.

At 48 h after sample preparation, the fibril length calculated from $\langle R_g^2\rangle_z^{1/2}$ is ~1500 nm, which is reasonably consistent with the lengths estimated from the micrographs. At longer time, however, there is no significant increase in $\langle R_g^2\rangle_z^{1/2}$, whereas Fig. 10 *C* shows extremely long fibrils of indeterminant length. Two factors are probably contributing to this apparent contradiction. First, the neglect of higher-order terms in q in deriving Eq. 2 becomes less valid as the particle size increases, leading to an underestimate of $\langle R_g^2\rangle_z^{1/2}$. Second, Eq. 3 is no longer appropriate as multifibril aggregates emerge which do not have a thin rodlike shape. For these aggregates, length increases much more rapidly than $\langle R_g^2\rangle_z^{1/2}$.

From both $\langle M\rangle_{w,app}$ and $\langle R_h\rangle_{z,app}$, a pattern of slow growth, then rapid growth, was seen. The ratio $\langle M\rangle_w/\langle M\rangle_n$ increased with time, suggesting an increase in the polydispersity of the mixture. $\langle R_h\rangle_{z,app}$ increased dramatically after ~150 h, whereas $\langle R_g^2\rangle_z^{1/2}$ remained approximately constant. This may be due in part to the breakdown in the assumptions of Eq. 2 as rod size increases, and the increasing importance of caging on the diffusivity. The data may also reflect a change in the structure of the aggregate, since the ratio $\langle R_h\rangle_z/\langle R_g^2\rangle_z^{1/2}$ would increase as the aggregate changed from an elongated to a more globular structure. This would occur as fibrils aggregate into bundles.The linear density $\langle M/L\rangle_w$ and the corresponding diameter $\langle d\rangle_w$ increased with time, with a more rapid increase after 120 h. Note that $\langle d\rangle_w$ is that of an equivalent cylindrical rod with the same linear density and does not necessarily correspond to the hydrodynamic diameter or to the diameter seen on the micrographs. The fact that $\langle d\rangle_w$ at early times is much less than the 10-nm diameter seen on the micrographs is a reflection of both the contribution of small oligomers, such as tetramers, to $\langle d\rangle_w$ and possibly a flat or hollow fibril structure.

We interpret these data as showing that fibril formation and elongation are the dominant processes occurring in the first 150 h, followed by fibril-fibril interaction afterwards. The rapid increase in size subsequent to 150 h is characteristic of the formation of a network of fibrils. We hypothesize that the early increase in $\langle M/L\rangle_w$ (before ~150 h) is due primarily to the coalescence of "protofibrils" into fibrils and that the later increase (~150–240 h) is due primarily to the formation of bundles of fibrils.

Upon dilution to 0.5 mg/ml, $\langle M\rangle_{w,app}$, $\langle M\rangle_{n,app}$, $\langle R_h\rangle_{z,app}$, $\langle R_g^2\rangle_z^{1/2}$ and $\langle M/L\rangle_w$ all decreased. $\langle M/L\rangle_w$ dropped by a factor of two, whereas $\langle M\rangle_{w,app}$ decreased by a factor of six. At 388 h, $\langle M\rangle_{w,app}$ is similar to that at 48 h, but $\langle R_g^2\rangle_z^{1/2}$ is much smaller and $\langle M/L\rangle_w$ is much larger. This suggests that fibril formation and/or fibril-fibril bundle formation are not entirely reversible over the time scales investigated. Both disentanglement of fibril bundles and fragmentation of individual fibrils may occur upon dilution. However, fibril-fibril interactions involve multiple contacts and are likely to be more resistant to dissociation than individual fibrils. This

concept would explain why the linear density of the aggregate at equivalent molecular mass is greater after dilution. A peptide solution made up fresh at 0.5 mg/ml concentration scattered light too weakly to measure any aggregation even after 7 days. This further supports the notion that aggregation of β(1–28) is under kinetic rather than thermodynamic control and that the sample history greatly influences the final outcome.

NaCl plays a significant role in fibril growth rates and fibril-fibril interactions. The importance of salt in self-assembly of β-sheet structures has been seen in other systems (Hilbich et al., 1991b; Zhang et al., 1993). QLS data show a remarkably greater rate of aggregation in the presence of physiological salt concentrations (Fig. 11 versus Fig. 8). Salt enhances fibril elongation, as evidenced by the generally longer fibrils seen in the micrograph taken at early time. $\langle\Gamma\rangle/q^2$ for samples C and D correspond to remarkably low diffusivities after 4–8 h. These diffusivities cannot be attributed to isolated fibrils. Instead, both caging and interfibrillary aggregation are likely explanations for these low diffusivities. We hypothesize that at high ionic strength fibril-fibril interactions occur very early on and are the major reason for the much greater rate of aggregation seen in the samples containing NaCl.

Electron micrographs taken after several weeks show two different patterns of fibril aggregates, depending on salt concentration. At the lower ionic strength, fibrils formed a mesh or network of entangled fibrils, with very little correlation of direction (Fig. 10 *C*). At the higher ionic strength, fibrils tended to align and form bundles (Fig. 10 *E*). Similar to our findings, Fraser et al. (1991a, 1992) reported that lateral aggregation of β(11–28) increased with increasing ionic strength. Nonrandom orientation of fibrils may occur simply due to hard core interactions at high concentrations. Keep and Pecora (1988) showed that a nonrandom orientation of rods must occur at $NL^2d > 2.26$, and may occur at lower values. If fibril length and/or fibril density is greater at the higher ionic strength, then hard-core interactions alone could account for the difference in fibril orientation. It should be noted that the maximum concentration for random orientation refers to the concentration of fibrils, but HPLC and gel electrophoresis data show that much of the peptide is not in fibrillar form. Thus, we suspect that the orientation of the fibrils at the high ionic strength is not due solely to packing considerations, but that attractive interfibrillary interactions play a role. A combination of electrostatic and hydrophobic interactions may account for these results. Repulsive electrostatic interactions at low ionic strength may cause the fibrils to maintain maximum interfibrillary distances and lead to a mesh-like network. At the higher ionic strength, electrostatic forces are more effectively screened and alignment could occur due to hydrophobic interactions which favor fibril-fibril interactions over fibril-solvent interactions.

Our experiments show, not surprisingly, that fibril formation is a strong function of concentration. At physiological pH and ionic strength, we saw no fibril formation at 0.2 mg/ml even after 9 days, but rapid and immediate fibril formation at concentrations of 0.5 mg/ml or greater, with the rate faster at the higher concentration. In this case, fibril formation occurred only at concentrations at which ThT and Congo red binding were detected. However, the opposite is not true. At the lower ionic strength, no fibril formation was detected by light scattering at 0.5 mg/ml concentration, even after 7 days incubation, despite the presence of ThT- and Congo red-binding species. This suggests that the presence of the hypothesized protofibrils is not in itself sufficient for fibril formation.

It is interesting to note that there are no short fibrils seen on the micrographs. One possible explanation is that fibril formation is autocatalytic, in that once a fibril starts to form, its elongation is very rapid. Alternatively, it could be due to difficulties in imaging shorter fibrils or protofibrils or washing off shorter fibrils from the grid. We suspect the latter is true for the following reason. The fibril density seen on the micrographs clearly increased dramatically with time, yet the peak areas (and presumably the concentration) of monomer and tetramer measured by HPLC did not change with time. One explanation that would be consistent with these data is that protofibrils are formed rapidly if the concentration is high enough, and these protofibrils, but not the tetramers or monomers, participate in the relatively slow process of fibril formation and elongation.

The appearance of a damped oscillatory autocorrelation function, which was seen at 240 h for sample A and 8 h for sample D, may be indicative of the strong correlations between fibrils that exist at this point. Oscillatory autocorrelation functions in other systems have been attributed to the onset of gelation and bulk motion of solvent and solute between two phases (Shukla et al., 1992). We did not see any macroscopic evidence of gelation or of phase separation in our systems; however, microgels may have formed. For the sample made by dilution from the TFA stock solution, measurements of the autocorrelation function (ACF) were continued after the initial appearance of the damped oscillatory ACF. The ACF signal weakened with time, whereas the total intensity did not change much. This may indicate that fibrils eventually form stiff entangled microgels, which contribute a static component to the scattering intensity.

It is clear from our data that a careful distinction must be made between solubility, fibril formation and elongation, interfibrillary aggregation, and phase separation when describing the physical properties of β(1–28). For example, despite clear evidence of amyloid fibril formation there was never any visible indication of loss of solubility. As another example, our data for sample A suggest that fibril formation is rapid and immediate, whereas there is a lag time for interfibrillary aggregation.

Sample preparation method influences fibril formation remarkably. Sample B was prepared by dissolving peptide first into the low ionic strength buffer used for sample A, then adjusting the salt concentration to that of sample D. Fibril growth rates for sample B were similar to sample A over the first 24 h. At later times, however, the aggregation behavior of sample B became more like sample D. For the sample

prepared from 0.1% TFA stock solution and diluted into PBSA, the size of the aggregates was similar to that for samples prepared by direct dissolution of lyophilized peptide into the same buffer. However, the number density was much lower, as evidenced by both the lower intensity of scattered light and the reduced number of fibrils on micrographs. Surprisingly, if the solution was prepared by diluting the TFA stock solution first into a low salt, then into a high salt buffer, no fibrils were detectable.

Our work clearly indicates that the aggregation mechanism of β(1–28) is very complex, and support the notion that the aggregation state is kinetically rather than thermodynamically determined. Sample preparation method, sample history, initial concentration, pH, ionic strength, time, and dilution all strongly affect the resulting aggregate concentration, size, and morphology. If the state of aggregation of the peptide is important in determining its toxicity, as has been suggested, than these factors must be carefully controlled for a realistic assessment of the in vivo and in vitro biological activity of β-amyloid peptide.

We thank Gary Parr for performing the mass spectroscopy, S. Damodaran for providing assistance in performing circular dichroism experiments, and Theresa Good for performing gel electrophoresis experiments and for a careful reading of the manuscript.

Funding was provided by Alzheimer's Disease Research, a program of the American Health Assistance Foundation.

REFERENCES

Barrow, C. J., and M. G. Zagorski. 1991. Solution structures of β peptide and its constituent fragments: relation to amyloid deposition. *Science (Wash. DC)*. 253:179–181.

Barrow, C. J., A. Yasuda, P. T. M. Kenny, and M. G. Zagorski. 1992. Solution conformations and aggregational properties of synthetic amyloid β-peptides of Alzheimer's disease. *J. Mol. Biol.* 225:1075–1093.

Burdick, D., B. Soreghan, M. Kwon, J. Kosmoski, M. Knauer, A. Henschen, J. Yates, C. Cotman, and C. Glabe. 1992. Assembly and aggregation properties of synthetic Alzheimer's A4/β amyloid peptide analogs. *J. Biol. Chem.* 267:546–554.

Castano, E. M., J. Ghiso, F. Prelli, P. D. Gorevic, A. Migheli, and B. Frangione. 1986. In vitro formation of amyloid fibrils from two synthetic peptides of different lengths homologous to Alzheimer's disease β-protein. *Biochem. Biophys. Res. Commun.* 141:782–789.

Chang, C. T., C. C. Wu, and J. T. Yang. 1978. Circular dichroic analysis of protein conformation: inclusion of the β-turns. *Anal. Biochem.* 91: 13–31.

Cohn, E. F., and J. T. Edsall. 1943. Proteins, Amino acids and Peptides. Reinhold Publishing Co., New York. p. 372.

Cotman, C. W., C. J. Pike, and A. Copani. 1992. β-Amyloid neurotoxicity: a discussion of in vitro findings. *Neurobiol. Aging.* 13:587–590.

Emre, M., C. Geula, B. J. Ransil, and M.-M. Mesulam. 1992. The acute neurotoxicity and effects upon cholinergic axons of intracerebrally injected β-amyloid in the rat brain. *Neurobiol. Aging.* 13:553–559.

Fraser, P. E., J. T. Nguyen, W. K. Surewicz, and D. A. Kirschner. 1991a. pH-dependent structural transitions of Alzheimer amyloid peptides. *Biophys. J.* 60:1190–1201.

Fraser, P. E., L. K. Duffy, M. B. O'Malley, J. Nguyen, H. Inouye, and D. A. Kirschner. 1991b. Morphology and antibody recognition of synthetic β-amyloid peptides. *J. Neurosci. Res.* 28:474–485.

Fraser, P. E., J. T. Nguyen, D. T. Chin, and D. A. Kirschner. 1992. Effects of sulfate ions on Alzheimer β/A4 peptide assemblies: implications for amyloid fibril-proteoglycan interactions. *J. Neurochem.* 59:1531–1540.

Games, D., K. M. Khan, F. G. Soriano, P. S. Keim, D. L. Davis, K. Bryant, and I. Lieberburg. 1992. Lack of Alzheimer pathology after β-amyloid protein injections in rat brain. *Neurobiol. Aging.* 13:569–576.

Geiduschek, E. P., and A. Holtzer. 1958. Application of light scattering to biological systems: deoxyribonucleic acid and the muscle proteins. *Adv. Biol. Med. Phys.* 6:431–551.

Glenner, G. G., and C. W. Wong. 1984. Alzheimer's disease: initial report of the purification and characterization of a novel cerebrovascular amyloid protein. *Biochem. Biophys. Res. Commun.* 120:885–890.

Gorevic, P. D., E. M. Castano, R. Sarma, and B. Frangione. 1987. Ten to fourteen residue peptides of Alzheimer's disease protein are sufficient for amyloid fibril formation and its characteristic X-ray diffraction pattern. *Biochem. Biophys. Res. Commun.* 147:854–862.

Hilbich, C., B. Kisters-Wolke, J. Reed, C. L. Masters, and K. Beyreuther. 1991a. Human and rodent sequence analogs of Alzheimer's amyloid βA4 share similar properties and can be solubilized in buffers of pH 7.4. *Eur. J. Biochem.* 201:61–69.

Hilbich, C., B. Kisters-Wolke, J. Reed, C. L. Masters, and K. Beyreuther. 1991b. Aggregation and secondary structure of synthetic amyloid βA4 peptides of Alzheimer's disease. *J. Mol. Biol.* 218:149–163.

Huglin, M. B. 1972. *In* Light Scattering from Polymer Solutions. M. B. Huglin, editor. Academic Press, New York. pp. 165–331.

Inouye, H., P. E. Fraser, and D. A. Kirschner. 1993. Structure of β-crystallite assemblies formed by Alzheimer β-amyloid protein analogues: analysis by x-ray diffraction. *Biophys. J.* 64:502–519.

Joachim, C. L., and D. J. Selkoe. 1992. The seminal role of β-amyloid in the pathogenesis of Alzheimer disease. *Alzheimer Dis. Assoc. Disord.* 6:7–34.

Kang, J., H.-G. Lemaire, A. Unterbeck, J. M. Salbaum, C. L. Masters, K.-H. Grzeschik, G. Multhaup, K. Beyreuther., and B. Muller-Hill. 1987. The precursor of Alzheimer's disease amyloid A4 protein resembles a cell-surface receptor. *Nature (Lond.)*. 325:733–736.

Keep, G. T., and R. Pecora. 1988. Dynamics of rodlike macromolecules in nondilute solutions: poly(*n*-alkyl isocyanates). *Macromolecules*. 21: 817–829.

Kirschner, D. A., H. Inouye, L. K. Duffy, A. Sinclair, M. Lind, and D. J. Selkoe. 1987. Synthetic peptide homologous to β protein from Alzheimer disease forms amyloid-like fibrils in vitro. *Proc. Natl. Acad. Sci. USA*. 84:6953–6957.

Klunk, W. E., J. W. Pettegrew, and D. J. Abraham. 1989a. Quantitative evaluation of Congo red binding to amyloid-like proteins with a beta-pleated sheet conformation. *J. Histochem. Cytochem.* 37:1273–1281.

Klunk, W. E., J. W. Pettegrew, and D. J. Abraham. 1989b. Two simple methods for quantifying low-affinity dye-substrate binding. *J. Histochem. Cytochem.* 37:1293–1297.

Koh, J.-Y., Yang, L. L., and C. W. Cotman. 1990. β-Amyloid protein increases the vulnerability of cultured cortical neurons to excitotoxic damage. *Brain Res.* 533:315–320.

Koo, E. H., L. Park, and D. J. Selkoe. 1993. Amyloid β-protein as a substrate interacts with extracellular matrix to promote neurite outgrowth. *Proc. Natl. Acad. Sci. USA*. 90:4748–4752.

Koppel, D. E. 1972. Analysis of macromolecular polydispersity in intensity correlation spectroscopy: the method of cumulants. *J. Chem. Phys.* 57: 4814–4820.

Kowall, N. W., M. F. Beal, J. Busciglio, L. K. Duffy, and B. A. Yankner. 1991. An in vivo model for the neurodegenerative effects of β amyloid and protection by substance P. *Proc. Natl. Acad. Sci. USA*. 88:7247–7251.

Kowall, N. W., A. C. McKee, B. A. Yankner, and M. F. Beal. 1992. In vivo neurotoxicity of beta-amyloid [β(1–40)] and the β(25–35) fragment. *Neurobiol. Aging.* 13:537–542.

Kuntz, I. D., Jr, and W. Kauzmann. 1974. Hydration of proteins and polypeptides. *Adv. Prot. Chem.* 28:239–245.

LeVine, H. 1993. Thioflavine T interaction with synthetic Alzheimer's disease β-amyloid peptides: detection of amyloid aggregation in solution. *Protein Sci.* 2:404–410.

Maeda, T., and S. Fujime. 1984. Spectrum of light quasielastically scattered from solutions of very long rods at dilute and semidilute regimes. *Macromolecules*. 17:1157–1167.

Malouf, A. T. 1992. Effect of beta amyloid peptides on neurons in hippocampal slice cultures. *Neurobiol. Aging.* 13:543–551.

Masters, C. L., G. Simms, N. A. Weinman, G. Multhaup, B. L. McDonald, and K. Beyreuther. 1985. Amyloid plaque core protein in Alzheimer

disease and Down syndrome. *Proc. Natl. Acad. Sci. USA.* 82:4245–4249.

Mattson, M. P., B. Cheng, D. Davis, K. Bryant, I. Lieberburg, and R. E. Rydel. 1992. β-Amyloid peptides destabilize calcium homeostasis and render human cortical neurons vulnerable to excitotoxicity. *J. Neurosci.* 12:376–389.

May, P. C., B. D. Gitter, D. C. Waters, L. K. Simmons, G. W. Becker, J. S. Small, and P. M. Robison. 1992. β-amyloid peptide in vitro toxicity: lot-to-lot variability. *Neurobiol. Aging.* 13:605–607.

Merz, P. A., H. M. Wisniewski, R. A. Somerville, S. A. Bobin, C. L. Masters, and K. Iqbal. 1981. An ultrastructural morphology of amyloid fibrils from neuritic and amyloid plaques. *Acta Neuropathol. (Berl.).* 60:113–124.

Naiki, H., K. Higuchi, M. Hosokawa, and T. G. Takeda. 1989. Fluorometric determination of amyloid fibrils in vitro using the fluorescent dye, thioflavine T. *Anal. Biochem.* 177:244–249.

Nicolai, T., and M. Mandel. 1989a. Ionic strength dependence of the second virial coefficient of low molar mass DNA fragments in aqueous solutions. *Macromolecules.* 22:438–444.

Nicolai, T., and M. Mandel. 1989b. Dynamic light scattering by aqueous solutions of low molar mass DNA fragments in the presence of NaCl. *Macromolecules.* 22:2348–2356.

Pike, C. J., A. J. Walencewicz, C. G. Glabe, and C. W. Cotman. 1991a. Aggregation-related toxicity of synthetic β-amyloid protein in hippocampal cultures. *Eur. J. Pharmacol.* 207:367–368.

Pike, C. F., A. J. Walencewicz, C. G. Glabe, and C. W. Cotman. 1991b. In vitro aging of β-amyloid protein causes peptide aggregation and neurotoxicity. *Brain Res.* 563:311–314.

Podlisny, M. B., D. T. Stephenson, M. P. Frosch, I. Lieberburg, J. A. Clemens, and D. J. Selkoe. 1992. Synthetic amyloid β-protein fails to produce specific neurotoxicity in monkey cerebral cortex. *Neurobiol. Aging.* 13:561–567.

Prelli, F. E. Castano, G. G. Glenner, and B. Frangione. 1988. Differences between vascular and plaque core amyloid in Alzheimer's disease. *J. Neurochem.* 51:648–651.

Provencher, S. W. 1982. A constrained regularization method for inverting data represented by linear algebraic or integral equations. *Comp. Phys. Commun.* 27:213–227.

Rozemuller, J. M., P. Eikelenboom, F. C. Stam, K. Beyreuther, and C. L. Masters. 1989. A4 protein in Alzheimer's disease: primary and secondary cellular events in extracellular amyloid deposition. *J. Neuropath. Exp. Neurol.* 48:674–691.

Rush, D. K., S. Aschmies, and M. C. Merriman. 1992. Intracerebral β-amyloid(25–35) produces tissue damage: is it neurotoxic? *Neurobiol. Aging.* 13:591–594.

Russo, P. S., F. E. Karasz, and K. H. Langley. 1984. Dynamic light scattering study of semidilute solutions of a stiff-chain polymer. *J. Chem. Phys.* 80:5312–5325.

Selkoe, D. J., M. B. Podlisny, C. L. Joachim, E. A. Vickers, G. Lee, L. C. Fritz, and T. Oltersdorf. 1988. β-Amyloid precursor protein of Alzheimer disease occurs as 110- to 135-kilodalton membrane-associated proteins in neural and nonneural tissue. *Proc. Natl. Acad. Sci. USA.* 85: 7341–7345.

Shukla, P., M. Muthukumar, and K. H. Langley. 1992. Dynamic light scattering studies of poly(γ-benzyl α,L-glutamate)benzyl alcohol system. *J. Appl. Polym. Sci.* 44:2115–2125.

Tomski, S. J., and R. M. Murphy. 1992. Kinetics of aggregation of synthetic β-amyloid peptide. *Arch. Biochem. Biophys.* 294:630–638.

Tracy, M. A., and R. Pecora. 1992. Dynamics of rigid and semirigid rodlike polymers. *Annu. Rev. Phys. Chem.* 43:525–527.

Waite, J., G. M. Cole, S. A. Frautschy, D. J. Connor, and L. J. Thal. 1992. Solvent effects on beta protein toxicity in vivo. *Neurobiol. Aging.* 13: 595–599.

Weyerich, B., B. D'Aguanno, E. Canessa, and R. Klein. 1990. Structure and dynamics of suspensions of charged rod-like particles. *Faraday Discuss. Chem. Soc.* 90:1–15.

Whitson, J. S., D. J. Selkoe, and C. W. Cotman. 1989. Amyloid β protein enhances the survival of hippocampal neurons in vitro. *Science (Wash. DC).* 243:1488–1490.

Wong, C. W., V. Quaranta, and G. G. Glenner. 1985. Neuritic plaques and cerebrovascular amyloid in Alzheimer disease are antigenically related. *Proc. Natl. Acad. Sci. USA.* 82:8729–8732.

Woody, R. W. 1985. Circular dichroism of peptides. *In* The Peptides: Analysis, Synthesis, Biology. V. J. Hruby, editor. Academic Press, Orlando, FL. 16–115.

Yamaguchi, H., Y. Nakazato, S. Hirai, M. Shoji, and Y. Hangaya. 1989. Electron micrograph of diffuse plaques. *Am. J. Pathol.* 135: 593–597.

Yamaguchi, H., Y. Nakazato, S. Hirai, and M. Shoji. 1990. Immunoelectron microscopic localization of amyloid β protein in the diffuse plaques of Alzheimer-type dementia. *Brain Res.* 508:320–324.

Yankner, B. A. 1992. Commentary and perspective on studies of beta amyloid neurotoxicity. *Neurobiol. Aging.* 13:615–616.

Yankner, B. A., L. K. Duffy, and D. A. Kirschner. 1990. Neurotrophic and neurotoxic effects of amyloid β protein: reversal of tachykinin neuropeptides. *Science (Wash. DC).* 250:279–282.

Zhang, S., T. Holmes, C. Lockshin, and A. Rich. 1993. Spontaneous assembly of a self-complementary oligopeptide to form a stable macroscopic membrane. *Proc. Natl. Acad. Sci. USA.* 90:3334–3338.